This is a postprint version of the following published document:

Morales-Céspedes, M., Paredes-Paredes, M.C., García Armada, A., Vandendorpe, L. (2017). Aligning the Light without Channel State Information for Visible Light Communications. *IEEE Journal on Selected Areas in Communications*, 36(1), pp. 91-105.

Aligning the Light without Channel State Information for Visible Light Communications

Máximo Morales-Céspedes, *Member, IEEE,*, Martha Cecilia Paredes-Paredes *Member, IEEE,* Ana García Armada, *Senior Member, IEEE*, and Luc Vandendorpe, *Fellow Member, IEEE*

Abstract—The use of light-emitting diodes (LED) for ambient illumination leads to visible light communications (VLC) as a promising technology for providing both constant lighting and high-speed wireless services in indoor environments. Since multiple LED sources can transmit to several users, this scenario naturally forms a multiple user multiple-input single-output (MU-MISO) system. In this sense, transmit precoding (TPC) schemes based on channel state information at the transmitter (CSIT) originally devised for radio-frequency (RF) systems have been proposed for their implementation in VLC. However, beyond providing CSIT or the need for cooperation among transmitters, which also result challenging in RF systems, there are several constraints such as the non-negativity of the transmitted signal or providing constant illumination that hamper the performance of TPC schemes in VLC. Taking into consideration these constraints, this paper explores the use of Blind Interference Alignment (BIA) for achieving multiplexing gain without CSIT or cooperation among LED lights. To do that, we devise the concept of reconfigurable photodetector that allows to switch among distinct and linearly independent channel responses. Simulation results show that the use of vBIA schemes based on the proposed reconfigurable photodetector results suitable for VLC systems.

Index Terms—Visible Light Communications, optical MIMO, precoding, blind interference alignment, reconfigurable photodetector, channel state information.

I. INTRODUCTION

Recently, visible light communications (VLC) have received significant attention as a means of moving part of the indoor wireless traffic, which is usually served through traditional radio frequency (RF) systems, to the wide and unregulated optical bandwidth of the radioelectric spectrum [1]. In indoor VLC systems, the use of light-emitting diodes (LEDs) for

providing illumination can be used for data transmission by modulating the optical intensity of the LEDs [2]. Since VLC offers several advantages such as a widespread deployment of LEDs, avoiding the interference with the traditional RF deployments or a low cost implementation, it is considered a promising technology for the fifth-generation (5G) of wireless communications and beyond [3].

In order to provide sufficient illumination several LED lamps are usually deployed in a single room [4]. Thus, the downlink for VLC deployments naturally configures a multi-user multiple-input single-output (MU-MISO) channel. From the network perspective the VLC systems can be considered as small cells integrated in a heterogeneous cellular network [5]. Notice that the VLC systems require to define a separated downlink and uplink, i.e., uplink transmission is not usually carried out through an optical channel [6]. In this sense, VLC systems will be placed within the coverage area of other radio access technologies (RAT) such as WiFi or femto/pico cells, which can be employed for uplink transmission. At this point, it is interesting to remark the importance of the backhaul links among the LED transmitters. Typically, the power-line has been considered for this issue, which results troublesome due to its dispersive and noisy nature. On the other hand, a solution such as the use of fiber-based backhaul links results unaffordable for low-cost deployments. Therefore, the design and integration of the downlink, uplink, and backhaul of the VLC systems within the framework of the 5G network is still an open challenge [6].

Although LED transmission does not interfere with RF, the VLC systems are subject to interference because of transmission from several LED sources to a set of users. Moreover, from a cellular perspective, the co-channel interference (CCI) is a significant factor for the degradation of the VLC cell performance when fractional frequency reuse (FR) is not considered [5]. Recently, transmit precoding (TPC) schemes based on knowledge of the Channel State Information at the Transmitter (CSIT) have been proposed for VLC systems for maximizing the Degrees of Freedom (DoF), i.e., the multiplexing gain, with respect to orthogonal approaches [7]. In [8], the use of Block Diagonalization (BD) precoding is proposed for VLC without considering the specific features of the optical systems. Similarly, a TPC scheme for minimizing the mean square error (MSE) is proposed in [9] taken into consideration the optical constraints of the VLC systems such as the non-negativity of the transmitted signal or providing constant illumination.

Beyond the aforementioned constraints, there exist several

issues that must be considered for the implementation of TPC schemes in VLC. First, accurate CSIT is required to obtain the precoding vectors at the transmitter side. Indeed, imperfect CSIT leads to a considerable performance degradation [10]. Moreover, notice that providing CSIT in VLC systems requires synchronization between the optical downlink and the umbrella RAT employed for uplink transmission. Secondly, and even more critical, cooperation among the LED transmitters would be required to apply these TPC schemes. Lastly, the optical channel responses can be highly correlated depending on the users distribution leading to a low performance of the TPC schemes [11].

Parallel to the development of VLC systems a novel transmission scheme referred to as Blind Interference Alignment (BIA) was proposed as a means of achieving a growth in DoF regarding the number of users without the need for CSIT [12]. BIA is based on exploiting a predefined pattern of channel correlations usually denoted as supersymbol. To generate these channel correlations the use of reconfigurable antennas for RF systems that can change their radiation pattern among a set of preset modes, which provide linear independent channel responses, is proposed in [13]. However, the implementation of BIA in RF systems demands high signal-to-noise ratio (SNR) due to the inherent noise increase of BIA and a coherence block large enough to consider the physical channel constant during the whole supersymbol transmission [14]. Although BIA schemes have been usually proposed for RF systems, they have not been considered for VLC to the best of our knowledge. At this point, it is interesting to remark several advantages that the combination of BIA and VLC systems could potentially provide

- VLC systems are characterized by high SNR, which allows to overcome the noise increase in BIA-based schemes.
- The optical wavelength is significantly smaller than the photodetector area. Therefore, the implementation of BIA schemes in VLC systems is not subject to small-scale fading effects.
- In contrast to TPC schemes, BIA does not require CSIT or cooperation among the LED transmitters.
- Transmission based on BIA ensures the non-negativity of the transmitted signal while providing constant illumination without DC bias constraints.

In this work we investigate the use of BIA for VLC systems motivated by the several advantages described above. However, the implementation of BIA in VLC is not straightforward. Although there exists a vast literature about reconfigurable antennas based on micro/nano electromechanical switches (MEMS/NEMS) or solid state switches [15], [16], this is not the case for VLC. The main contribution of this paper is the design of a reconfigurable photodetector able to provide linearly independent channel entries for each preset mode. After describing the structure of the reconfigurable photodetector we define the use of BIA in VLC systems referred to as vBIA. Furthermore, there exist several BIA schemes for partially connected cellular networks that avoid the use of FR to cancel the CCI [17], [18]. We describe the use
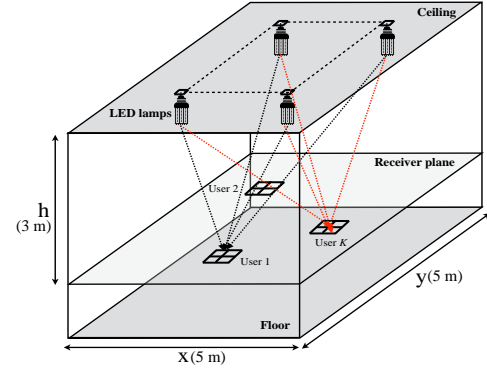

Fig. 1. Multi-user MIMO indoor VLC system.

of BIA in VLC cell environments showing the resilience of vBIA in amorphous cellular formations defined by the network topology [7]. Simulations results show that vBIA provides satisfactory user rates outperforming other schemes based on multichannel receivers without CSIT such as maximum ratio combining (MRC) [5]. In comparison with the TPC scheme of [9] based on CSIT, which achieves greater peak user rates, vBIA avoids the blackspot areas because of the constraints of the optical channel providing a more fair distribution of the user rate.

The remainder of this paper is organized as follows. In Section II the system model for VLC with reconfigurable photodetectors is described. The VLC set-up comprising the LED transmission, the optical channel and the configuration of the reconfigurable photodetector is defined in Section III. In Section IV we present the BIA scheme for fully connected VLC systems and Section V shows the use of BIA schemes in other VLC topologies such as homogeneous and heterogeneous deployments of light sources. Section VII presents some simulation results where the performance of vBIA is compared to MRC and a TPC scheme. Finally, Section VIII provides concluding remarks.

II. SYSTEM MODEL

We consider an indoor VLC system consisting of L, $t = \{1, \ldots, L\}$, LED lamps that transmit data to K, $k = \{1, \ldots, K\}$, terminal users while providing constant illumination as is shown in Fig. 1. Each user is equipped with a reconfigurable photodetector, a concept that is described below, able to provide L distinct and linearly independent channel responses referred to as preset modes. The signal transmitted by the set of LEDs can be written in a vector form as $\mathbf{x} = [x_1, \ldots, x_L]^T \in \mathbb{R}_+^{L \times 1}$. Thus, the signal received by the user k at time slot n is given by

$$y^{[k]}[n] = |\mathbf{h}^{[k]}\left(\nu^{[k]}[n]\right)^T | \mathbf{x}[n] + z^{[k]}[n], \qquad (1)$$

where $\mathbf{h}\left(\nu^{[k]}[n]\right) \in \mathbb{R}_+^{L \times 1}$ is the channel vector between the L LED transmitters and the user k for the preset mode ν selected at time n and $z^{[k]}[n]$ is real valued additive white Gaussian noise with zero mean and variance $\sigma_z^2 = \sigma_{shot}^2 + \sigma_{thermal}^2$ where σ_{shot}^2 is the shot noise variance and $\sigma_{thermal}^2$ is the thermal noise variance [19], [20].

We assume that the set of LED transmitters do not have any CSIT. On the contrary, the selection switching pattern functions $\nu^{[k]}[n]$ are known beforehand and each transmitter does not have more information than the coherence time. Furthermore, there do not exist coordination or data sharing among the LED transmitters. For the sake of simplicity, we focus on the temporal dimension without loss of generality and each symbol extension corresponds to a time slot. Nevertheless, all the results can be easily applied to the frequency domain.

III. VISIBLE LIGHT COMMUNICATIONS SET-UP

A. Transmitter

For VLC systems, the LED lamps are employed for both providing indoor illumination and data transmission. In this context, the particular characteristics of LED data transmission yield several constraints in comparison with the RF transmission schemes. First, the signal transmitted by the LEDs must be a non-negative real value. Notice that this constraint results critical for TPC schemes since negative values of the transmitted signal are usually required to cancel the interference. Moreover, the output optical power is only linear over a limited drive current range $[I_L, I_H]$ where I_L is the turn on current of the LED and I_H corresponds to the maximum input that ensures both the linear response of the LED and the human eye safety. Within this range, each LED provides an output power $[0, P_{max}]$. Secondly, in order to provide a constant lighting the optical fluctuation must be high enough to guarantee a variation above the fusion frequency of the human eye, from which only the average of the optical signal is perceived.

Typically, a set of LED lights is considered for providing illumination. For data transmission this configuration can be considered as a multiple input channel. We consider that the information to the user k is modulated through a pulse amplitude modulation (PAM) with mean equal to the current that provides the desired illumination intensity. Therefore, the average of the transmitted signal must remain constant over the time in order to provide a stable brightness, i.e., $\mathbb{E}\left\{\|\mathbf{x}[t]\|\right\} = P_{avg}$ where P_{avg} is the average output optical power [21].

B. Channel

The VLC channel can be described as a flat fading channel or a diffused channel depending on the propagation conditions. According to [22], [23] the channel gain between the LED transmitter t and the photodiode ν of the user k at time n is given by

$$\eta_t^{[k]}(\nu, n) = \eta_{\text{LOS},t}^{[k]}(\nu)\delta(n) + \eta_{\text{diff}}(n - \Delta T), \qquad (2)$$

where $\eta_{\text{LOS},t}^{[k]}$ is the Line-of-Sight (LOS) component, η_{diff} is the contribution due to Non-LOS (NLOS) diffuse reflections and ΔT is the delay between the LOS and NLOS components.

The LOS component depends directly on the Euclidian distance between the user k and the LED transmitter t denoted by d_{kt}. Assuming that each user is equipped with L

photodiodes, the angle of irradiance and the angle of incidence for the photodiode ν, $\nu = \{1, \ldots, L\}$, are denoted as ϕ_{kt} and $\varphi_{kt}(\nu)$[1], respectively, as is shown in Fig. 2. The LOS component between the LED transmitter t and the user k at preset mode ν, defined as DC gain [19], is

$$\eta_{\text{LOS},t}^{[k]}(\nu) =$$
$$\begin{cases} \frac{\gamma A}{d_{kt}^2} R_0\left(\phi_{kt}\right) T_{eq}\left(\varphi_{kt}(\nu)\right) \cos^r\left(\varphi_{kt}(\nu)\right) & \text{if } \varphi_{kt}(\nu) \leq \Psi_c \\ 0 & \text{if } \varphi_{kt}(\nu) \geq \Psi_c \end{cases}$$
$$(3)$$

where γ denotes the responsivity coefficient and A is the physical area of the photodiode. For the preset mode ν, $T_{eq}\left(\varphi_{kt}(\nu)\right) = T\left(\varphi_{kt}(\nu)\right) g\left(\varphi_{kt}(\nu)\right)$ is the optical response of the filter and concentrator lens where $T\left(\varphi_{kt}(\nu)\right)$ is the gain of the optical filter, $g\left(\varphi_{kl}(\nu)\right)$ is the gain of the optical concentrator and r is the coefficient of the photodiode associated to the field-of-view (FOV) angle Ψ_c [24]. Moreover, in (3) $R_0\left(\phi_{kl}\right)$ denotes the Lambertian radiation intensity $R_0 = \frac{m+1}{2\pi} \cos^m\left(\phi\right)$, where m is the order of Lambertian emission. The order m is related to the transmitter semiangle $\phi_{1/2}$ by $m = \frac{-\ln 2}{\ln(\cos(\phi_{1/2}))}$.

The diffuse component in the frequency domain is [22]

$$h_{\text{diff}}(f) = \frac{\eta_{\text{diff}}}{1 + j\frac{f}{f_d}} \qquad (4)$$

where f_d is the -3 dB cut-off frequency of the diffuse optical channel and $\eta_{\text{diff}} = \frac{A}{A_{\text{room}}} \cdot \frac{\rho_1}{1-\rho}$, where recall that A is area of detection of the photodiode, A_{room} is the area of the room surface, ρ_1 is the reflectivity of the region initially illuminated by the LED lights and ρ is the average reflectivity of the walls. Similarly to other works, we consider $\rho_1 = \rho$ [22], [23].

To complete the characterization of the VLC channel we consider the limited modulation bandwidth of the LED transceivers. The normalized impulse response of the LED is denoted as $\eta_{\text{LED}}(n)$ and its frequency response modeled as $h_{\text{LED}}(f) = e^{-\frac{f}{1.44f_m}}$, where f_m is the -3 dB modulation bandwidth of the LED [23]. Thus, the VLC channel impulse response at the photodiode ν of the user k can be written as

$$\eta_{\text{eq},t}^{[k]}(\nu, n) = \left(\eta_{\text{LOS},t}^{[k]}(\nu) + \eta_{\text{diff}}\left(n - \Delta T\right)\right) * \eta_{\text{LED}}(n), \quad (5)$$

which channel impulse response in the frequency domain is

$$h_t^{[k]}(\nu, f) = \left(\eta_{\text{LOS},t}^{[k]}(\nu) + \eta_{\text{diff}}\frac{e^{j2\pi\Delta T}}{1 + j\frac{f}{f_d}}\right) e^{-\frac{f}{1.44f_m}}. \qquad (6)$$

The reflectivity index of the visible light on the wall is about $\rho = 0.4$. Moreover, as in [23] we consider a cut-off frequency of the diffuse channel of $f_d = 30$ MHz and a delay between the LOS and NLOS components of $\Delta T = 20$ ns. Therefore, according to [22] we can conclude that the channel gain is almost flat for frequencies under the cut-off frequency of the diffuse optical channel. Thus, assuming that this condition is

---

[1]Considering that the photodiodes of each user are within a physical area much smaller than the distance to any LED transmitter the angle of irradiance between each photodiode of the user k and the transmitter t can be approximated as $\phi_{kt}(\nu) \approx \phi_{kt}$.
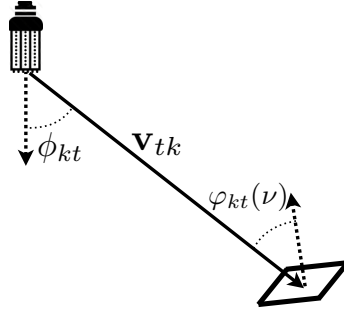
Fig. 2. Geometry of the irradiance and incidence angles for the transmitter-receiver pair.

Fig. 3. Orientation vector of a photodiode (face) of the pyramidal photodetector.

satisfied, the channel gain can be written as

$$h_t^{[k]}(\nu) = \left(\eta_{\text{LOS},t}^{[k]}(\nu) + \eta_{\text{diff}}\right) e^{-\frac{f}{1.44 f_m}}. \tag{7}$$

C. Receiver

We introduce the concept of reconfigurable photodetector inspired by the reconfigurable antennas for RF systems [15]. Basically, a reconfigurable photodetector provides a set of linearly independent channel responses. Similarly to the angle-diversity receivers [19], we consider a receiver equipped with multiple photodiodes for achieving multiplexing gain without CSIT.

Let us assume receivers equipped with at least L photodiodes[2] where each user selects the signal from a photodiode of the whole set of L photodiodes at each time slot as a preset mode. In contrast to the RF reconfigurable antennas, which provide L preset modes connected to a unique RF chain, the proposed reconfigurable photodetector provides L outputs connected to a unique signal processing chain as is shown in Fig. 4. Similarly to other works, e.g., [25], we consider a dedicated area for allocation of the L photodiodes in the layout of each receiver. Specifically, we consider a volume of dimensions 18.5 mm×18.5 mm×9.25 mm for the photodiodes section assuming photodiodes with an area of detection equals to 15 mm². Each photodiode is connected to a transimpedance amplifier (TIA). Currently, there exist several architectures for signal detection that obtain great performance for VLC requirements of data rate comprising a small size [26]. Moreover, these components of the reconfigurable photodetector results economically affordable. In this sense, notice that the complexity of the signal detection of the L photodiodes is similar to other multichannel receivers.

Considering L LED transmitters and a reconfigurable photodetector providing L preset modes we can define the channel matrix of the user k as

$$\mathbf{H}^{[k]} = \begin{bmatrix} \mathbf{h}^{[k]}(1)^T \\ \mathbf{h}^{[k]}(2)^T \\ \vdots \\ \mathbf{h}^{[k]}(L)^T \end{bmatrix} = \begin{bmatrix} h_1^{[k]}(1) & h_2^{[k]}(1) & \dots & h_L^{[k]}(1) \\ h_1^{[k]}(2) & h_2^{[k]}(2) & \dots & h_L^{[k]}(2) \\ \vdots & & & \vdots \\ h_1^{[k]}(L) & h_2^{[k]}(L) & \dots & h_L^{[k]}(L) \end{bmatrix},$$

$$\tag{8}$$

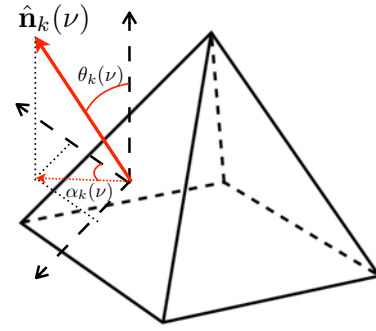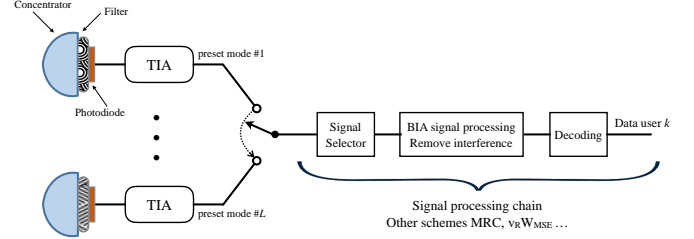[2]More than L photodiodes could be considered for providing diversity or improving the FOV.

Fig. 4. Structure of the receiver based on the proposed reconfigurable photodetector.

where $h_t^{[k]}(\nu)$, $\nu \in \{1, 2, \dots, L\}$, is the channel response between the LED transmitter t and the user k at preset mode ν given by (3). For a spatial deployment of LED lamps, which ensures distinct radiation angle from each LED transmitter, the design of the filter and the concentrator of each photodiode that compose a reconfigurable photodetector aims to provide linear independent responses. In the following we describe two methodologies to obtain linearly independent responses, i.e., a set of preset modes, for the proposed reconfigurable photodetector.

Remark 1. *The use of optical receivers composed of several photodiodes has been typically proposed for providing diversity through schemes such as MRC [5]. In these sense, the multiple outputs of the reconfigurable photodetector can be used for implementing these schemes.*

1) Filter and concentrator design: Optical filters and concentrators are usual components in the photodiode receivers and they are presented in most of the commercial optical systems.

For thin-film plane filters [27] the optical gain given by a generic angle of incidence φ is

$$T(\varphi; \Delta\lambda, \hat{\varphi}) = \frac{T_0}{1 + \left[\frac{\lambda_0 - \lambda(\varphi; \hat{\varphi})}{\frac{\Delta\lambda}{2}}\right]^{2m}} \tag{9}$$

where T_0 corresponds to the peak transmission, λ_0 is the wavelength of the transmitted signal, $\frac{\Delta\lambda}{2}$ is the spectral half-power bandwidth and $\lambda(\varphi; \hat{\varphi})$ represents the shifting to shorter wavelengths at non-normal incidences, which is given by $\lambda(\varphi, \hat{\varphi}) = \lambda_0 \left(\frac{n_s^2 - n_1^2 \sin^2 \varphi}{n_s^2 - n_1^2 \sin^2 \hat{\varphi}}\right)$, where n_s and n_1 are the
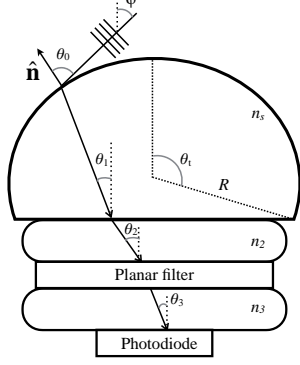
Fig. 5. Structure of a spherical lens.

Fig. 6. Optical gain of different lens structures.

effective index of the spacer layer and input layer, respectively, and $\hat{\varphi}$ is the filter orientation. Notice that the parameters n_s, m, and T_0 can be handled to obtain different channel responses.

To obtain wide FOV and optical gain truncated spherical lenses are usually proposed for VLC systems [27]. As can be seen in Fig. 5, the light incides over a spherical lens with a truncation angle θ_t forming an angle θ_0 with the normal of the lens surface. Hence, the single ray cross the lens surface attenuated by a factor $T(\theta_0)$. After that the ray is reflected with an angle θ_1. In this way, $T(\theta_1)$, $T(\theta_2)$ and $T(\theta_3)$ corresponds to the gain given by the lens output, the planar filter (if any) and the photodiode input, respectively. In this case, the optical gain of the lens is

$$g(\varphi) = \frac{\int_{S_0} T(\theta_0)T(\theta_1)T(\theta_2)T(\theta_3)dS}{\int_{S_0} \cos(\theta_0)dS}, \qquad (10)$$

where S_0 is the integration area over the surface for which light passing through eventually hits the photodiode. For the sake of simplicity we focus on hemispherical lenses with $\theta_t = 90°$. An idealized hemispherical concentrator with an intern reflective index n_s achieves a gain

$$g(\varphi) = \begin{cases} \frac{n_s^2}{\sin^2 \Psi_c} & \text{if } 0 \le \varphi \le \Psi_c \\ 0 & \text{if } \varphi \le \Psi_c. \end{cases} \qquad (11)$$

Notice that narrow FOVs increase the optical gain of the concentrator lens. There are a vast literature of filter structures, e.g., planar, spherical, coated, etc., that provide distinct and linearly independent responses for the same angle of incidence [27]. In Fig. 6 we show the optical gain for different lens structures with the angle of incidence. It can be seen that linearly independent responses, i.e., preset modes of the reconfigurable photodetector, can be obtained by simply varying the structure of the set composed of the concentrator and the filter of each photodiode.

2) Geometrical angle receiver design: The orientation of each photodiode of the reconfigurable photodetector can be employed for creating an angle diversity receiver where each orientation vector corresponds to a preset mode as is shown in Fig. 3. Therefore, varying the angle of incidence through the orientation of each photodiode it is possible to obtain linearly independent responses for the same angle of irradiance.
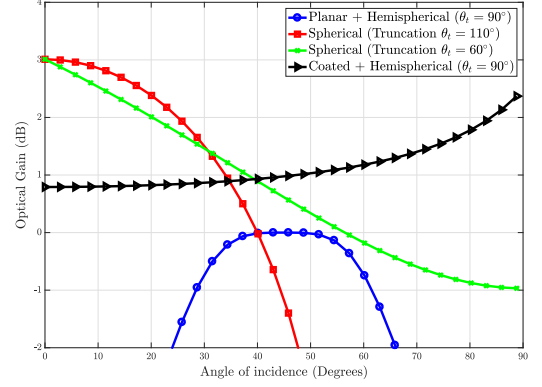
Assuming that the photodiode ν of the reconfigurable photodetector of user k obtains distinct polar and azimuthal angles on the x-y planed denoted as $\theta_k(\nu)$ and $\alpha_k(\nu)$, respectively, the orientation vector of the photodiode ν of user k is given by

$$\hat{\mathbf{n}}_k = $$
$$[\sin(\theta_k(\nu))\cos(\alpha_k(\nu)), \sin(\theta_k(\nu))\sin(\alpha_k(\nu)), \cos(\theta_k(\nu))] \qquad (12)$$

Thus, the irradiance and the incidence angle can be easily determined by

$$\phi_{kt} = \arccos\left(\frac{\hat{\mathbf{n}}_t \cdot \mathbf{v}_{tk}}{\|\hat{\mathbf{n}}_t\|\|\mathbf{v}_{tk}\|}\right) \qquad (13)$$

$$\varphi_{kt}(\nu) = \arccos\left(\frac{\mathbf{v}_{kt} \cdot \hat{\mathbf{n}}_k(\nu)}{\|\mathbf{v}_{kt}\|\|\hat{\mathbf{n}}_k(\nu)\|}\right), \qquad (14)$$

respectively, where $\hat{\mathbf{n}}_t$ is the normal vector of the LED transmitter t and $\mathbf{v}_{kt}$ is the vector from the LED transmitter t and the user k as is shown in Fig. 2.

Following the design proposed in [25], we consider an angle diversity receiver where the photodiodes are pointing to different directions such as the triangle faces of a pyramid as is shown in Fig. 3. For a pyramid receiver, the photodiodes are located in a circle of radius r_{PD} on the horizontal plane over a receiver height h_{PD}. Thus, assuming L photodiodes at each receiver, the position of the photodiode corresponding to the preset mode ν, $\nu = \{1, \dots, L\}$, is

$$(x_k(\nu), y_k(\nu), z_k(\nu)) =$$
$$\left(x_k + r_{PD}\cos\frac{2(\nu-1)\pi}{L}, y_k + r_{PD}\sin\frac{2(\nu-1)\pi}{L}, h_{PD}\right) \qquad (15)$$

Therefore, the orientation of the photodiode that provides the preset mode ν of the user k is given by the polar and azimuth angles denoted as $\theta_k(\nu) = \theta_k$ and $\alpha_k(\nu) = \frac{2(\nu-1)\pi}{L}$, respectively.

IV. BLIND INTERFERENCE ALIGNMENT FOR VISIBLE LIGHT COMMUNICATIONS

In this section we describe the BIA scheme applied to VLC systems, which is referred to as vBIA. Each receiver
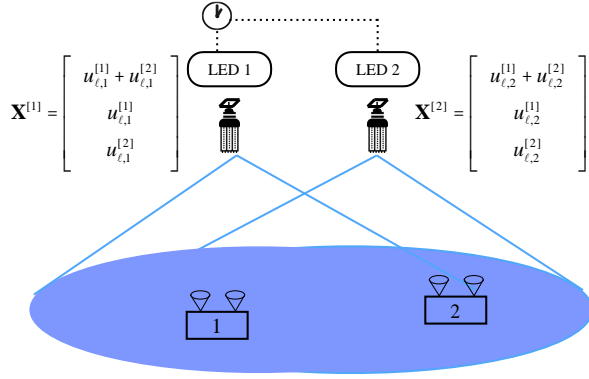
Fig. 7. VLC scenario equivalent to a MISO BC with $L = 2$ LED transmitters and $K = 2$.

	1	2	3
User 1	$\mathbf{h}^{[1]}(1)$	$\mathbf{h}^{[1]}(2)$	$\mathbf{h}^{[1]}(1)$
User 2	$\mathbf{h}^{[2]}(1)$	$\mathbf{h}^{[2]}(1)$	$\mathbf{h}^{[2]}(2)$

Fig. 8. Supersymbol of vBIA for a MISO BC with $L = 2$ LED lights and $K = 2$ users. Each color represents a preset mode.

is equipped with the proposed reconfigurable photodetector described in Section III-C. With the aim of introducing the principles of BIA applied to VLC systems, we focus on the pattern of signal selection of the reconfigurable photodetector for the MISO BC proposed in [13] where the whole set of LED transmitters is connected to all the users.

A. Toy example

For illustrative purposes, consider first a toy example with $K = 2$ users and $L = 2$ LED transmitters as is shown in Fig. 7. Assuming full connectivity between the LED lights and the users, this scenario can be considered as a MISO BC for the vBIA scheme. Thus, each LED transmitter sends a data stream to each user. Notice that, assuming orthogonal resource allocation in absence of CSIT such as TDMA, transmitting 2 independent data streams free of interference from both LED lights to each user involves 4 time slots, i.e., the sum-DoF equals 1.

Following the scheme of [13] the optimal DoF, i.e., the multiplexing gain, without CSIT can be achieved by considering a frame comprising 3 symbol extensions[3] denoted as *supersymbol*. During the supersymbol each user follows the preset mode selection of the reconfigurable photodetector described in Fig. 8. The signal transmitted by the LED transmitter t during the 3 symbol extensions can be written in a vector form as

$$\mathbf{X}^{[t]} = \begin{bmatrix} u_{t,\ell}^{[1]} + u_{t,\ell}^{[2]} & u_{t,\ell}^{[1]} & u_{t,\ell}^{[2]} \end{bmatrix}^T, \quad (16)$$

[3]In this work we focus on the temporal dimension and therefore, each symbol extension corresponds to a time slot.

where $u_{t,\ell}^{[k]}$ is the symbol transmitted by the LED light t to the user k, $\ell = 1$ for this particular case. Thus, the user k desires to decode the symbol $\mathbf{u}_\ell^{[k]} = \begin{bmatrix} u_{1,\ell}^{[k]}, u_{2,\ell}^{[k]} \end{bmatrix}^T$, which contains 2 DoF. Hence, the signal transmitted by the set of LED lights can be written as

$$\mathbf{X} = \mathbf{X}^{[1]} + \mathbf{X}^{[2]} = \begin{bmatrix} \mathbf{x}[1] \\ \mathbf{x}[2] \\ \mathbf{x}[3] \end{bmatrix} = \begin{bmatrix} \mathbf{I}_2 \\ \mathbf{I}_2 \\ \mathbf{0}_2 \end{bmatrix} \mathbf{u}_\ell^{[1]} + \begin{bmatrix} \mathbf{I}_2 \\ \mathbf{0}_2 \\ \mathbf{I}_2 \end{bmatrix} \mathbf{u}_\ell^{[2]}, \quad (17)$$

where $\mathbf{x}[n] \in \mathbb{C}^{2 \times 1}$ is the signal transmitted during the symbol extension n and $\mathbf{I}_2$ and $\mathbf{0}_2$ denote the 2×2 identity and zero matrix, respectively.

Before analyzing the interference cancellation through vBIA, it is interesting to remark some properties of the proposed transmission strategy. First, note that the precoding of the desired symbol (see (17)) only considers adding operations of zeros and one values. Therefore, in contrast to the TPC schemes, the non-negativity of the signal is guaranteed without the need for a bias current. Furthermore, as can be checked in (16), each LED light transmits an independent data stream to both users without the need for cooperation or data sharing among the LED transmitters. That is, the symbols $u_{\ell,t'}^{[k]}$, $t' = \{1, ..., L\} : t' \neq t$, are unknown by the LED transmitter t. Only some synchronization would be required.

Taking into consideration the pattern of preset mode selection of the supersymbol shown in Fig. 7 and the structure of the signal transmitted, the signal received at user 1 can be written as

$$\begin{bmatrix} y^{[1]}[1] \\ y^{[1]}[2] \\ y^{[1]}[3] \end{bmatrix} = \underbrace{\begin{bmatrix} \mathbf{h}^{[1]}(1)^T \\ \mathbf{h}^{[1]}(2)^T \\ \mathbf{0}_2 \end{bmatrix}}_{\text{rank}=2} \mathbf{u}_1^{[1]} + \underbrace{\begin{bmatrix} \mathbf{h}^{[1]}(1)^T \\ \mathbf{0}_2 \\ \mathbf{h}^{[1]}(1)^T \end{bmatrix}}_{\text{rank}=1} \mathbf{u}_1^{[2]} + \begin{bmatrix} z^{[1]}[1] \\ z^{[1]}[2] \\ z^{[1]}[3] \end{bmatrix}.$$
$$(18)$$

Notice that the desired symbol $\mathbf{u}_1^{[1]}$, which carries 2 DoF, is contained in a $\text{rank} - 2$ matrix while the interference is aligned in a $\text{rank} - 1$ matrix, i.e., the interference is aligned into a one-dimensional space. As a consequence, the user 1 can employ the third symbol extension to measure and cancel the interference caused by the transmission of $\mathbf{u}_1^{[2]}$ during the first symbol extension. Furthermore, the signal received by user 1 is free of interference during the second symbol extension. After subtracting the interference the received signal for user 1 is

$$\begin{bmatrix} y^{[1]}[1] - y^{[1]}[3] \\ y^{[1]}[2] \end{bmatrix} = \begin{bmatrix} \mathbf{h}^{[1]}(1)^T \\ \mathbf{h}^{[1]}(2)^T \end{bmatrix} \mathbf{u}_1^{[1]} + \begin{bmatrix} z^{[1]}(1) - z^{[1]}(3) \\ z^{[1]}(2) \end{bmatrix}.$$
$$(19)$$

Since the interference is completely removed and the proposed reconfigurable photodetector provides linearly independent channel responses for $\mathbf{h}^{[1]}(\nu)$, $\nu = \{1, 2\}$, the 2 DoF contained in the symbol $\mathbf{u}_1^{[1]}$ are decodable by solving the linear problem (19). Similarly, the user 2 can decode the 2 DoF of $\mathbf{u}_1^{[2]}$ over the symbol extensions $\{1, 3\}$ and measuring the interference due to transmission $\mathbf{u}_1^{[1]}$ at symbol extension 2. Therefore, 4 symbols are decodable during a supersymbol comprising 3 symbol extensions. That is, $\frac{4}{3}$ DoF are achievable without CSIT or cooperation between the LED transmitters by

using vBIA.

B. General case

1) Design of the supersymbol structure: As described in [13], the BIA supersymbol must satisfy two conditions; (i) Ensure the decodability of the L independent data streams transmitted by each of the L LED lights to user k by varying its channel state among L distinct preset modes of the reconfigurable photodetector during the L symbol extensions where the desired symbol $\mathbf{u}_\ell^{[k]} = \left[u_{1,\ell}^{[k]}, \ldots, u_{L,\ell}^{[k]} \right]^T$, which contains L DoF, is transmitted. Notice that this condition guarantees to obtain a full rank matrix after interference subtraction (see (19)) and therefore, decode the L DoF carried by $\mathbf{u}_\ell^{[k]}$. (ii) The channel state of all other users $k' \neq k$ must remain constant during the transmission of $\mathbf{u}_\ell^{[k]}$ to the user k. This condition allows to contain the interference because of transmission of $\mathbf{u}_\ell^{[k]}$ in a single preset mode for all other users. Satisfying these conditions for a MISO BC with L LED transmitters and K users requires $(L-1)^{K-1}$ blocks comprising L symbol extensions for each user denoted as *alignment blocks*. An alignment block for the user k is defined as the set of L symbol extensions where the channel state of this user varies among L preset modes while all other users maintain a constant channel state.

Furthermore, the BIA supersymbol can be divided into two well differentiated sections; Block 1 where the symbols to all the users are simulatenously transmitted, and therefore, generating multi-user interference, and Block 2 where each symbol $\mathbf{u}_\ell^{[k]}$ is transmitted in orthogonal fashion. This structure allows to measure the symbols transmitted to other users, $\mathbf{u}_\ell^{[k']}$, $k' \neq k$, in Block 2 and subtract it afterwards from the symbol extensions of Block 1 polluted by it when the interference is properly aligned as described in detail in Section IV-B3. The first $L-1$ symbol extensions of the alignment block of each user belong to Block 1 where the symbols to all users are transmitted simultaneously. At this point, let us define the first $L-1$ symbol extensions of each alignment block of the user k as a *group* for this user. Therefore, the Block 1 of the supersymbol can be assembled by considering groups as is shown in Fig. 9. This procedure is mathematically described in detail in [13]. Since each group belongs to a specific alignment block, it can be seen in Fig. 9 that each group comprises $L-1$ distinct channel states while all other users remain in a constant channel state. As commented above, simultaneous transmission to all users occurs during the $L-1$ symbol extensions of each alignment block, i.e., during a group. Since $(L-1)^{K-1}$ alignment blocks are required to satisfy the BIA conditions, the Block 1 comprises $(L-1) \times (L-1)^{K-1} = (L-1)^K$ symbol extensions.

Once the Block 1 has been defined the Block 2 is composed of the last symbol extension of each alignment block. Since orthogonal transmission of each symbol $\mathbf{u}_\ell^{[k]}$ occurs during the Block 2, it comprises $K(L-1)^{K-1}$ symbol extensions. Therefore, the length of the supersymbol comprises $(L-1)^K + K(L-1)^{K-1}$ symbol extensions.

2) Design of the precoding matrices and signal transmission in Block 1: Once the structure of Block 1 is defined, the
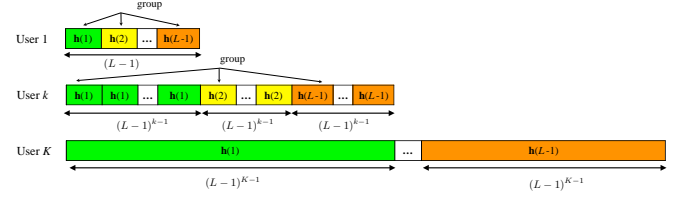

Fig. 9. The structure of Block 1 for the vBIA scheme. User indexes are removed from the channel responses for simplicity. Each color represents a preset mode.

design of the precoding matrices can be easily determined. Let us denote $\mathbf{u}_\ell^{[k]} = \left[u_{1,\ell}^{[k]}, \ldots, u_{L,\ell}^{[k]} \right]$, as the symbol transmitted during the alignment block ℓ, $\ell = \left\{ 1, \ldots, (L-1)^{K-1} \right\}$, which carries L distinguishable streams, where $u_{t,\ell}^{[k]}$ is the contribution of the LED light t, $t = \{1, \ldots, L\}$. Taking into consideration the structure of Block 1, the symbol $\mathbf{u}_\ell^{[k]}$ is repeatedly transmitted during the group of its ℓ-th alignment block, i.e., during the first $L-1$ symbol extensions of that alignment block. Notice that transmission of $\mathbf{u}_\ell^{[k]}$ during Block 1 generates interference to all other users, which maintain a constant channel state during its transmission in order to align the inference. For instance, considering the structure shown in Fig. 9, the symbol $\mathbf{u}_1^{[1]}$ to user 1 is transmitted during the first $L-1$ symbol extensions of the supersymbol where its channel state varies among $L-1$ distinct preset modes $\left\{ \mathbf{h}^{[1]}(\nu) \right\}_{\nu=1}^{L-1}$. Notice that all other users select the preset mode $\mathbf{h}^{[k']}(1)$, $k' \neq 1$, during the first $L-1$ symbol extensions. Following this methodology the symbol $\mathbf{u}_1^{[k]}$ to the user k is transmitted during the symbol extension $\left\{ m(L-1)^{k-1} + 1 \right\}_{m=0}^{L-1}$. Furthermore, transmission between the $(L-1)^{K-1}$ alignment blocks of each user must be orthogonal to avoid the overlapping with each other. As described in detail in [13], the precoding matrix for the user k consists of marking with a $L \times L$ identity matrix within the column corresponding to the ℓ-th alignment block the positions where the group corresponding to the symbol $\mathbf{u}_\ell^{[k]}$ is located in the supersymbol.

3) Transmission in Block 2 and interference cancellation: Recall that the first $L-1$ symbol extensions of each alignment block are already determined by Block 1 and the precoding structure described above. Thus, the last symbol extension that completes each alignment block is provided by Block 2. Therefore, in order to ensure the decodability of the L streams carried by $\mathbf{u}_\ell^{[k]}$ the user k selects the preset mode L, i.e., $\mathbf{h}^{[k]}(L)$, during its transmission in Block 2.

As can be seen in Fig. 10, the Block 2 can be divided in K parts where the symbols $\mathbf{u}_\ell^{[k]}$, $\ell = \{1, \ldots, (L-1)^{K-1}\}$, are orthogonally transmitted to the user k. Due to the orthogonal transmission all other users $k' \neq k$ can measure the interference received in Block 1 because of transmission of the symbols $\mathbf{u}_\ell^{[k]}$, $\ell = \{1, \ldots, (L-1)^{K-1}\}$. Since the interference is aligned according to the two conditions described in Section IV-B1, the users $k' \neq k$ can measure the interference because of transmission of $\mathbf{u}_\ell^{[k]}$ in Block 2 at the same preset mode as it interferes in Block 1. To do that, the preset mode selected by the user k' during the transmission of $\mathbf{u}_\ell^{[k]}$ in Block
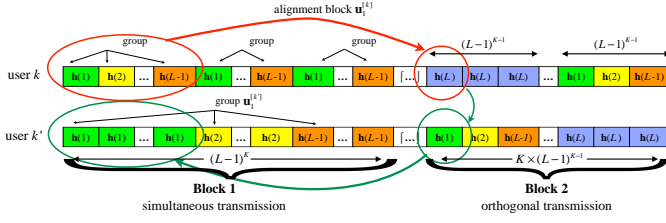
Fig. 10. Construction of the Block 2 for the vBIA scheme and interference measurement and subtraction. Each color represents a preset mode
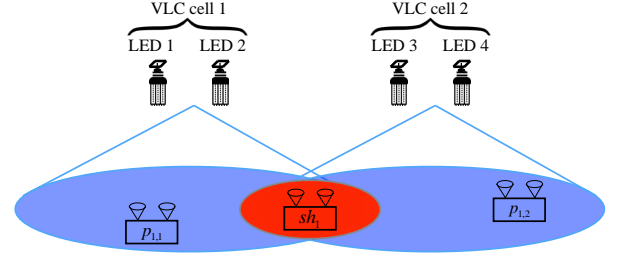

Fig. 11. Partially connected scenario. The LED transmitters are grouped in VLC cells composed of $L_c = 2$ lamps and there exist $K_p = 1$ private users per cell and $K_{sh} = 1$ shared user that receives a strong signal from the whole set of LED lights.

2 must coincide with the preset mode selected in Block 1 during the group of user k where the symbol $\mathbf{u}_\ell^{[k]}$ is transmitted as is shown in Fig. 10.

For example, in Fig. 10, the first $L-1$ symbol extension of the supersymbol form a group that composed an alignment block with the first symbol extensions of the Block 2 in which the symbol $\mathbf{u}_1^{[k]}$ is transmitted. Since the symbol $\mathbf{u}_1^{[k]}$ is transmitted orthogonally by the L LED lights, the user k' can measure at the preset mode $\mathbf{h}^{[k']}(1)$ the interference received during the first $L-1$ symbol extensions of Block 1 due to transmission of $\mathbf{u}_1^{[k]}$.

4) Achievable Degrees of Freedom: Since each of the K users achieves L DoF in each of its $(L-1)^{K-1}$ alignment blocks over a supersymbol comprising $(L-1) \times (L-1)^{K-1} = (L-1)^K$ symbol extensions, the sum-DoF per symbol extension achieved by the vBIA scheme equals

$$\text{DoF} = \frac{LK(L-1)^{K-1}}{(L-1)^K + K(L-1)^{K-1}} = \frac{LK}{L+K-1}, \quad (20)$$

which corresponds to the optimal sum-DoF without CSIT [13]. Interestingly, the sum-DoF tends to the optimal assuming CSIT as the number of users grows. That is, $\lim_{K \to \infty} \frac{LK}{L+K-1} = L$.

Remark 2. *The implementation of BIA schemes is subject to transmission of the supersymbol within a coherence time period and a noise increase because of the interference subtraction [14]. In this sense, typical VLC settings result in supersymbol lengths short enough to consider the optical channel constant during its transmission and provide an operating SNR enough to get through the noise increase. However, for non-usual settings with a large number of LED transmitters, a large number of users or high mobility indoor environment several BIA schemes based on the methodology described in Section IV-B such as [14], [28] have been proposed for managing both the supersymbol length and the noise increase. By using the reconfigurable photodetector devised in Section III-C these schemes can be implemented for VLC systems.*

V. MOVING TO OTHER NETWORK TOPOLOGIES

Until now, we have focused on a uniform scenario where all the users are connected to the whole set of LED transmitters. However, the propagation of the visible light is usually confined in a small area. Thus, the deployment of several LED lamps in an indoor scenario naturally leads to network topologies defined by the connectivity of the users [6]. For VLC traditional management of the network topology such as frequency reuse (FR) involves a loss in DoF because of

the partial connectivity given by the small area of coverage of the LED lights. Moreover, FR involves switching between VLC frequencies every few meters. Supported by the concept of reconfigurable photodetector derived in Section III-C, BIA can provide a user-centric approach determined by the network topology, e.g., [17], [18], [28], jointly to the several advantages described previously such as low requirement for backhaul links or non-negativity of the transmitted signal. The aim of this section is not the development of these BIA schemes, that are already reported in the literature, but to highlight the versatility of BIA applied to VLC.

A. Homogeneous partially connected networks

Assuming an indoor deployment of several LED lamps we consider the concept of VLC cell composed of one or more LED transmitters proposed in [6]. Thus, for homogeneous deployments as is shown in Fig. 11, each user can be categorized either as a *private user* receiving a strong signal from a unique VLC cell or a *shared user* that receives a useful signal from the whole set of LED transmitters. This kind of partially connected networks can be modeled by the BIA scheme devised in [17] based on the network topology.

For illustrative purposes, we first consider a partially connected network as is shown in Fig. 11 where there exist $L = 4$ LED lamps that can be grouped in $C = 2$, $c = \{1, 2\}$, VLC cells composed of $L_c = 2$ transmitters each. Moreover, each VLC cell transmits to $K_p = 1$ private user while a $K_{sh} = 1$ shared user is served by both cells. Assuming a fully connected network the channel of the user k, either private or shared, at the preset mode ν can be written as

$$\mathbf{h}^{[k]}(\nu) = \begin{bmatrix} h_1^{[k]}(\nu) & h_2^{[k]}(\nu) & h_3^{[k]}(\nu) & h_4^{[k]}(\nu) \end{bmatrix} \in \mathbb{R}_+^{4 \times 1} \tag{21}$$

However, taking into consideration the partial connectivity of the VLC network and the aforementioned categorization, the channel of the private users after some relabelling can be written as $\mathbf{h}^{[p_{1,1}]}(\nu) = \begin{bmatrix} h_1^{[p_{1,1}]}(\nu) & h_2^{[p_{1,1}]}(\nu) & 0 & 0 \end{bmatrix}$ and $\mathbf{h}^{[p_{1,2}]}(\nu) = \begin{bmatrix} 0 & 0 & h_3^{[p_{1,2}]}(\nu) & h_4^{[p_{1,2}]}(\nu) \end{bmatrix}$ for the private users of the VLC cells 1 and 2 denoted as $p_{1,1}$ and $p_{1,2}$, respectively[4]. Similarly, the channel of

---

[4]The channel vector $\mathbf{h}^{[p_{1,c}]}(\nu)$ does not consider the interference because of transmission by the VLC cell $c' \neq c$ since this influence is treated, and therefore computed, as noise.
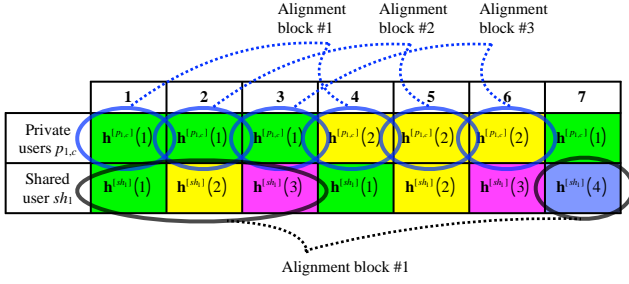
Fig. 12. Supersymbol structure for a partially connected network comprising 2 VLC cells composed of 2 LED transmitters. Each VLC cell transmits to $K_p = 1$ private users while a $K_{sh} = 1$ shared user is served by both VLC cells. Each color represents a preset mode.
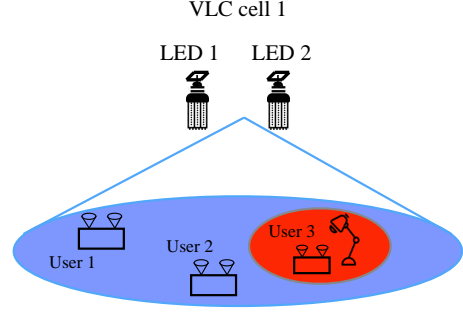

Fig. 13. Heterogeneous deployment for VLC. The LED lamps provide illumination and data transmission and a reading light transmits to a specific user improving the lighting in a small area.
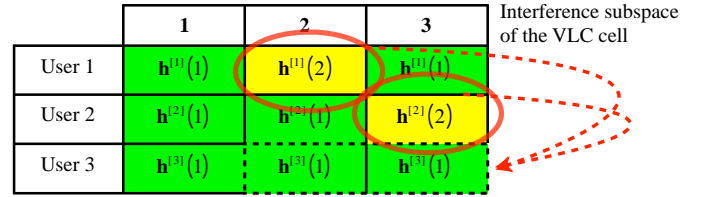

Fig. 14. Supersymbol for cogBIA where 2 LED lamps provide illumination and transmit to 2 users while a reading light serves to a specific user. Each color represents a preset mode.

the shared user can be relabelled as $\mathbf{h}^{[sh_1]}(\nu) = \left[h_1^{[sh_1]}(\nu) \quad h_2^{[sh_1]}(\nu) \quad h_3^{[sh_1]}(\nu) \quad h_4^{[sh_1]}(\nu) \right]$. Therefore, it can be easily seen from (8) that the channel matrix for the private users is $\mathrm{rank} - 2$ while the shared user obtains a $\mathrm{rank} - 4$ channel matrix. By using this approach it is possible to reorganize the pattern of preset mode selection to exploit the partial connectivity of the VLC network instead of considering it as a handicap. First, note that transmission to the private users in cell c does not interfere to the private users of the neighbouring cells $c' \neq c$ while transmission to the shared user interferes to both private users. Thus, the supersymbol structure of the private users can be reused by each cell while ensuring the alignment with the shared user.

For the considered setting the supersymbol of the topological vBIA is as shown in Fig. 12. It can be seen that each private user obtains 3 alignment blocks formed by the symbol extensions $\{1, 4\}$, $\{2, 5\}$ and $\{3, 6\}$ aligned at the preset modes $\mathbf{h}^{[sh_1]}(1)$, $\mathbf{h}^{[sh_1]}(2)$ and $\mathbf{h}^{[sh_1]}(3)$ of the shared user, respectively. Each of these alignment blocks provides 2 DoF according to the rank of the channel matrix of the private users. Moreover, the shared user obtains an alignment block at symbol extensions $\{1, 2, 3, 7\}$ aligned at the preset mode $\mathbf{h}^{[p_{1,c}]}(1)$ of the private users.

Then, following the proposed topological approach each private user achieves 3 alignment blocks with 2 DoF each while the shared user located between both VLC cells obtains 4 DoF in a single alignment block by exploiting the partial connectivity of the scenario. Therefore, $\frac{2 \times 3 \times 2 + 4}{7} = \frac{16}{7} \approx 2.28$ DoF are achievable in the considered setting. Curiously, assuming full connectivity and applying vBIA as described in Section IV for $L = 4$ LED transmitters and $K = 3$ users 2 DoF are achievable (see (20)), i.e., $\frac{2}{7}$ less than the vBIA topological approach. This toy example leads to an interesting fact; *the lack of connectivity in a VLC network can be treated as a resource instead of a handicap that allows to obtain more DoF than schemes based on full connectivity without CSIT or cooperation among the LED transmitters.*

For general partially connected networks the construction of the supersymbol structure and the precoding matrices is explained in detail in [17]. Assuming L LED transmitters grouped in C VLC cells formed by L_c LED lamps each, i.e., $L = C \times L_c$, where each VLC cell transmits to K_p private users and there are K_{sh} shared users served by the whole

set of LED transmitters, the achievable sum-DoF per symbol extension of the VLC system is

$$\mathrm{DoF}_{\mathrm{topBIA}} = \frac{L \left[K_{sh}(L_c - 1) + K_p(L - 1) \right]}{(L - 1)(L_c - 1) + K_{sh}(L_c - 1) + K_p(L - 1)}, \tag{22}$$

which corresponds to the optimal DoF for partially connected networks in absence of CSIT [17].

B. Heterogeneous partially connected networks

Indoor deployments of LED lamps usually follow an homogeneous distribution. However, it is easy to formulate heterogeneous deployments where a small source of light is interfered by a bigger VLC cell as is shown in Fig. 13, e.g., a reading lamp within an indoor VLC deployment. Assuming absence of CSIT or cooperation among the LED transmitters the straightforward solution would be to divide the transmission resources, e.g., split the available bandwidth and assigning each slice to each cell. However, supported by the reconfigurable photodetector devised in this work, more efficient schemes based on cognitive BIA can be employed.

For illustrative purposes consider a heterogeneous network as is shown in Fig. 13 where the users 1 and 2 are served by a VLC cell composed of 2 LED lamps while the user 3 is served by a reading light that provides a small lighting area contained within the VLC cell. Following [18], the supersymbol structure is as shown in Fig. 14. Notice that the switching pattern of the users 1 and 2 corresponds to the supersymbol of the MISO BC (see Fig. 8). Since the users 1 and 2 are not subject to

interference from the reading light, they can use the BIA scheme described in Section IV-A. Assuming that the signal transmitted by the VLC cell equals (17), the reading light transmits $u^{[3]}$ during the first symbol extension, where $u^{[3]}$ is the symbol desired by the user 3 carrying 1 DoF, while it remains in silent during the following 2 symbol extensions[5].

For the user 3 served by the reading light decoding $u^{[3]}$ is subject to interference because of transmission of the VLC cell. At this point, note that BIA schemes transmit the interference subspace of the VLC cell at user 3 during the Block 2 of the considered supersymbol. By taking advantage of this structure, the interference received during the reception of $u^{[3]}$ at the first symbol extension can be measured at symbol extensions 2 and 3 by simply ensuring that the reading light remains in silent in a cognitive fashion and subtracting it afterwards. After interference subtraction the signal received by user 3 is

$$y^{[3]}[1] - \left(y^{[3]}[2] + y^{[3]}[3] \right) = h^{[3]}(1)u^{[3]}. \qquad (23)$$

Thus, the user 3 can decode 1 DoF during 3 symbol extensions without any penalty for the users served by the VLC cell, which achieve 2 DoF during the entire supersymbol. As a result, for the considered setting the use of BIA obtains $\frac{5}{3}$ DoF. It is worth to remark that orthogonal approaches without CSIT are limited to 1 DoF in the whole system, i.e., $\frac{2}{3}$ DoF less than the proposed BIA approach for the considered setting.

The key idea behind the cognitive BIA approach is to exploit the structure of the BIA supersymbol in heterogeneous networks. Considering a VLC cell as an upper tier, the signal space because of transmission to its users comprises the Block 2 of the supersymbol structure. Therefore, a smaller source of light whose users are subject to interference from an upper tier can take advantage of this structure for measuring the interference space of the upper tier by simply remaining silent in a cognitive fashion during the Block 2 of the interfering VLC cell. Notice that this cognitive BIA approach can be implemented using any BIA scheme.

VI. ACHIEVABLE RATES

In this section, we show the achievable rates of a generic vBIA scheme. Without loss of generality, consider a generic alignment block for a user k with connectivity to L LED transmitters. Following a BIA scheme, the user k can remove the interference received during the first $L-1$ symbol extensions of the ℓ-th alignment block because of simultaneous transmission to $K_i - 1$ users during Block 1. Notice that $K_i - 1$ refers to the number of interference terms that must be subtracted. Thus, the signal of the user k after interference subtraction in the alignment block ℓ, which carries the symbol

$\mathbf{u}_\ell^{[k]}$, can be written as

$$\tilde{\mathbf{y}}^{[k]} = \begin{bmatrix} \tilde{y}^{[k]}[1] \\ \vdots \\ \tilde{y}^{[k]}[L-1] \\ \tilde{y}^{[k]}[L] \end{bmatrix} = \begin{bmatrix} \mathbf{h}^{[k]}(1)^T \\ \vdots \\ \mathbf{h}^{[k]}(L-1)^T \\ \mathbf{h}^{[k]}(L)^T \end{bmatrix} \mathbf{u}_\ell^{[k]}$$
$$+ \begin{bmatrix} z^{[k]}[1] - \sum_{j=1,j\neq k}^K z^{[k]}[j] \\ \vdots \\ z^{[k]}[L-1] - \sum_{j=1,j\neq k}^K z^{[k]}[j] \\ z^{[k]}[L] \end{bmatrix}. \qquad (24)$$

where for simplicity the temporal index refers to the symbol extension in the alignment block instead of referring to the position in the supersymbol. As can be seen, each user can decode the L DoF of $\mathbf{u}_\ell^{[k]}$ by solving a $L \times L$ equation system given by

$$\tilde{\mathbf{y}}^{[k]} = \mathbf{H}^{[k]}\mathbf{u}_\ell^{[k]} + \tilde{\mathbf{z}}^{[k]}, \qquad (25)$$

where

$$\mathbf{H}^{[k]} = \left[\mathbf{h}^{[k]}(1)^T \quad \mathbf{h}^{[k]}(2)^T \quad \dots \quad \mathbf{h}^{[k]}(L)^T \right]^T \in \mathbb{R}^{L \times L} \qquad (26)$$

is the channel matrix of the user k, which is assumed to be full rank and highly uncorrelated because of the entries of the proposed reconfigurable photodetector, and $\tilde{\mathbf{z}}^{[k]} \sim \mathcal{CN}\left(0, \sigma_z^2 \mathbf{R}_{\tilde{\mathbf{z}}}\right)$ is the noise vector after the interference subtraction where

$$\mathbf{R}_{\tilde{\mathbf{z}}} = \begin{bmatrix} K_i \mathbf{I}_{L-1} & \mathbf{0} \\ \mathbf{0} & 1 \end{bmatrix}. \qquad (27)$$

Besides, the ratio of alignment blocks per user over the entire supersymbol denoted as B_r must be taken into consideration. For instance, in a fully connected scenario as considered in Section IV each user obtains $(L-1)^{K-1}$ alignment blocks over the entire supersymbol. That is, $B_r = \frac{(L-1)^{K-1}}{\mathcal{L}_{SS}} = \frac{1}{L+K-1}$. This ratio can be easily obtained for other BIA schemes. Thus, the normalized rate per symbol extension of the user k can be written as [13], [29]

$$R^{[k]} = B_r \, \mathbb{E}\left[\log \det \left(\mathbf{I} + P_{str}\mathbf{H}^{[k]}\mathbf{H}^{[k]^T}\mathbf{R}_z^{-1} \right) \right] \qquad (28)$$

where P_{str} is the power allocated to each data stream. Given the constraints of a VLC system, constant power allocation during the entire supersymbol is assumed for providing constant illumination, i.e., same power allocation during Block 1 and Block 2. Furthermore, focused on the data transmission, this approach results optimal regarding other power allocation schemes, e.g., uniform power allocation to each symbol [29].

VII. SIMULATION RESULTS

We now present the numerical results for characterizing the performance of the vBIA scheme based on the proposed reconfigurable photodetector. Specifically, we consider a reconfigurable photodetector with $L = 4$ preset modes arranged in a pyramidal geometry and equipped with an hemispherical concentrator lens each. For comparison purposes we also consider the use of the L photodiodes of the reconfigurable photodetector for providing diversity through a MRC scheme [5]

---

[5]For data transmission above the fusion frequency of the human eye, this condition does not involve blinking of the illumination.

or multiplexing gain by implementing the TPC scheme of [9]. For this TPC scheme we consider two approaches; (i) each user employs the signal received from the L photodiodes of its reconfigurable photodetector[6] referred to as $v_R W_{MSE}$ and (ii) a single-photodetector approach as in [9] with a detection area equal to the area of the L photodiodes referred to as $v_D W_{MSE}$. The setup of the VLC system comprises $L = 4$ LED lights in two different scenarios. The scenario A considers a uniform distribution of the LED lights in a $5 \times$m 5m$\times$3m room at the positions $[1.5, 1.5, 3]$, $[1.5, 3.5, 3]$, $[3.5, 1.5, 3]$ and $[3.5, 3.5, 3]$ as described in Fig. 1. The scenario B is a corridor with size of 2m$\times 12$m$\times 3$m where the LED transmitters are located at the positions $[1, 2, 3]$, $[1, 3, 3]$, $[1, 7, 3]$ and $[1, 8, 3]$. The users are randomly distributed over the plane $h = 2.15$ m away from ceiling and they are equipped with a pyramidal photodetector with $L = 4$ faces tilted $30°$ each. In order to provide uniform illumination the optical power of each LED lamp is within the range $(-4, 16)$ dBW [30]. If it is not specified, an optical power of 10 dBW is considered. The other parameters of the proposed VLC system are listed in Table I.

TABLE I
PARAMETERS OF THE VLC SYSTEM

Parameter	Value
Number of LED transmitters L	4
Detector responsivity γ	0.53 A/W
Bandwidth BW	20 MHz
Refractive index of the filter n_s	1.5
Physical area of the photodiode A	15 mm^2
Gain of optical filter T_0	1.0
Transmitter semi-angle $\phi_{1/2}$	70deg
Noise power spectral density [20] σ_z^2	10^{-22}A^2/Hz
Receiver FOV Ψ_c	60deg
LED modulation cut-off frequency [23] f_m	30 MHz

Following we show the distribution of the achievable user rate for vBIA, MRC, and $v_R W_{MSE}$ in the scenario A. It is interesting to remark that the position of all other users does not affect to the rate of a specific user for these schemes. For vBIA it can be seen that the parameters B_r and $\mathbf{R_{\tilde{z}}}$ depend only on the number of users while the channel matrix $\mathbf{H}^{[k]}$ is independent for each user (see (28)). On the other hand, orthogonal resource allocation is considered for avoiding the multi-user interference for MRC. Similarly, $v_R W_{MSE}$ transmits L data streams to the L photodiodes of each user in each time slot avoiding the influence of all other users.

For $K = 2$ users, it can be seen in Fig. 15 that the proposed vBIA scheme provides a user rate above 100 Mbps in most of the areas of the scenario. Moreover, the peak user rate is obtained in the center and decreases moderately as the user moves to the corners. In contrast, in Fig. 16 the MRC

[6]Since each user is equipped with a reconfigurable photodetector with the same number of photodiodes as LED transmitters, $\min\{L, KL\} = L$ DoF can be achieved per symbol extension by CSIT-based schemes. Therefore, orthogonal approaches are required for serving each user in a dedicated symbol extension in which the user obtains L DoF. Notice that given this orthogonal approach the user performance does not depend on the position of all other users.

scheme only provides user rates above 100 Mbps within areas close to each LED light due to the influence of the intercell interference. Therefore, extremely low values of user rate are obtained in the center of the scenario. In Fig. 17, it can be seen that $v_R W_{MSE}$ achieves a considerable higher peak user rate than vBIA or MRC in the center of the scenario. However, the user rate is extremely low with respect to the peak user rate in some areas of the scenario referred to as blackspots from now on. These blackspot areas are given by the influence of the constraints imposed by the optical channel for TPC schemes.

The distributions of the user rate for $K = 4$ achieved by vBIA, MRC and $v_R W_{MSE}$ in the scenario A are depicted in Fig. 18, Fig. 19 and Fig. 20, respectively. It can be seen that the shape of the user rate distribution is quite similar as for the $K = 2$ case. However, the user rate achieved by $v_R W_{MSE}$ is half of the values achieved with $K = 2$. On the other hand, the penalization of serving $K = 4$ users is only around the 35% regarding the $K = 2$ users case for vBIA providing a user rate above 65 Mbps in most of the scenario. The MRC scheme is not heavily penalized by the user increase since only users served by the same LED light are transmitted orthogonally. However, the user rate is heavily subject to intercell interference.

The average of the achievable user rate with the optical power of each LED light in the scenario A for vBIA, MRC, $v_R W_{MSE}$ and $v_D W_{MSE}$ is depicted in Fig. 21 for $K = 4$ users. First, notice that in contrast to the other schemes the achievable user rate of MRC is almost constant as the optical power increases since it is subject to intercell interference. Besides, since $v_R W_{MSE}$ and $v_D W_{MSE}$ obtains the same multiplexing gain, i.e., $\min(L, KL) = L$ DoF, it can be seen that the user rate increases with the same slope. However, the need for orthogonal user allocation penalizes $v_R W_{MSE}$ in comparison with $v_D W_{MSE}$. The vBIA scheme achieves a similar average user rate in the whole scenario as $v_D W_{MSE}$ within the range of $(2, 10)$ dBW. As the optical power increases it can be seen that $v_D W_{MSE}$ outperforms vBIA.

Although both TPC schemes, $v_R W_{MSE}$ and $v_D W_{MSE}$ can achieve high values of peak user rate, they are subject to the inherent constraints given by the properties of the optical channel. As a consequence, a user can obtain a low rate when the channel responses are correlated or these constraints are hard to satisfy. With the aim of determining the variation of the user rate for each transmission scheme we show the Jain fairness index [31] obtained for an optical power of 10 dBW in scenario A. It can be seen that vBIA achieves the most fair user rate, i.e., each user obtains similar rate independently of its position. Similarly, MRC guarantee that all users obtains a minimum rate. However, both TPC schemes achieve a lower fairness index in comparison with vBIA. As a conclusion, vBIA provides a more uniform user rate distribution in comparison with TPC schemes, which generate blackspots where the user rate is extremely low.

In Fig. 22 we plot the average BER for $K = 2$ and $K = 4$ users with the optical power of each LED light when a 2-PAM is considered for data transmission. It is interesting to remark that MRC obtains a BER floor at $4 \cdot 10^{-2}$ when the optical power is beyond 6 dBW. This BER floor is due to
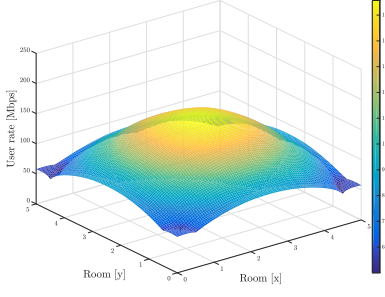
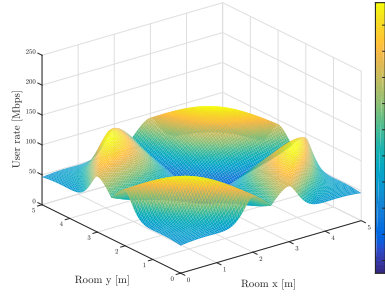Fig. 15. Distribution of the user rate for vBIA. Scenario A, $K = 2$.

Fig. 16. Distribution of the user rate for MRC. Scenario A, $K = 2$.
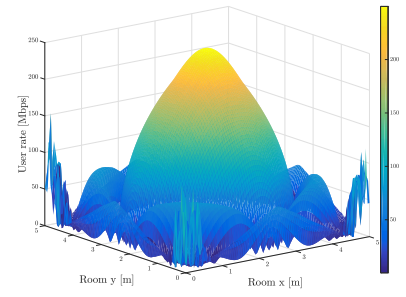

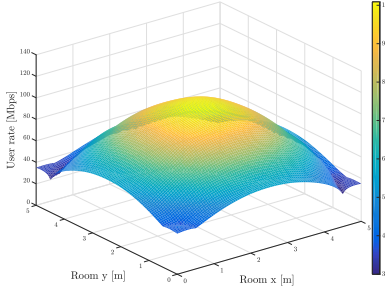Fig. 17. Distribution of the user rate for $v_R W_{MSE}$. Scenario A, $K = 2$.

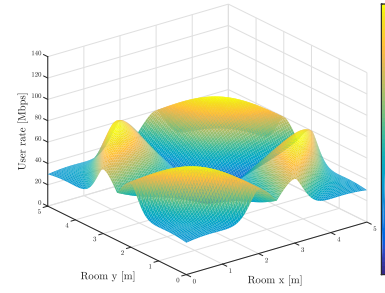Fig. 18. Distribution of the user rate for vBIA. Scenario A, $K = 4$.

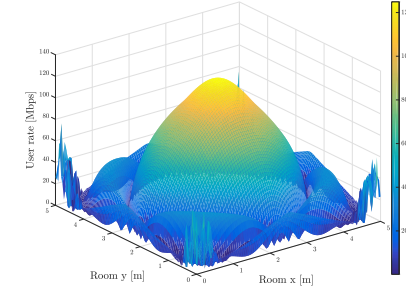Fig. 19. Distribution of the user rate for MRC. Scenario A, $K = 4$.

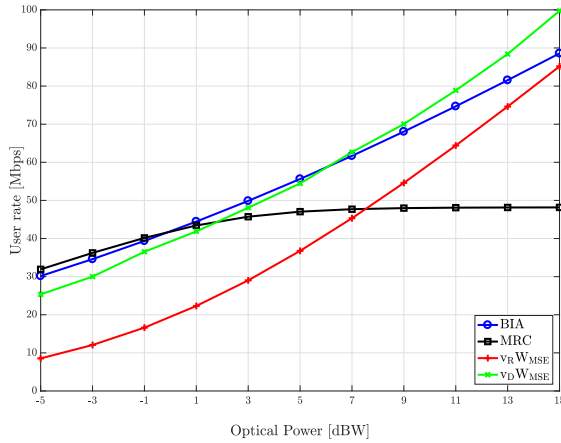Fig. 20. Distribution of the user rate for $v_R W_{MSE}$. Scenario A, $K = 4$.

Fig. 21. Average user rate in the scenario A for vBIA, MRC, $v_R W_{MSE}$ and $v_D W_{MSE}$. $K = 4$.

TABLE II
JAIN FAIRNESS INDEX FOR VBIA, MRC, $v_R W_{MSE}$ AND $v_D W_{MSE}$ IN THE SCENARIO A

	vBIA	MRC	$v_R W_{MSE}$	$v_D W_{MSE}$
Jain index	0.94	0.84	0.61	0.65

intercell interference, which is not managed for MRC. The proposed vBIA scheme obtains a BER below 10^{-5} and 10^{-3} for $K = 2$ and $K = 4$, respectively, at an optical power of 10 dBW. For $K = 2$, the $v_D W_{MSE}$ scheme obtains a lower BER than vBIA in the power range from -4 dBW to

6 dBW. However, for $K = 4$ the $v_D W_{MSE}$ scheme obtains a worse BER in the whole optical power range. Thus, the proposed vBIA achieves satisfactory BER within the power range for providing indoor illumination. Notice that the vBIA and the $v_D W_{MSE}$ schemes have different sources of error as the number of users increases. The vBIA scheme suffers a noise enhancement due to interference subtraction (see (27)) while the increase of users leads to higher correlation among the channel entries for $v_D W_{MSE}$. By using the proposed reconfigurable photodetector, the $v_R W_{MSE}$ scheme achieves a BER with a similar slope as $v_D W_{MSE}$ for $K = 2$. Hence, the use of reconfigurable photodetectors can handle the channel correlation for TPC schemes in VLC.

The achievable user rate of vBIA for homogeneous cellular VLC networks is shown in Fig. 23. For the scenario B, the LED lamps at the positions $\{2, 3.5\}$ m and $\{8.5, 10\}$ m in the y-axis compose the VLC cells 1 and 2, respectively. Considering the topological approach proposed in Section V-A the VLC cells provide a user rate above 60 Mbps within an area comprising 3.5 m approximately. However, out of this coverage area the user rate decreases abruptly and the private user turns into a shared user. In contrast, a user rate above 50 Mbps can be guaranteed in the blackspot between both VLC cells for the topological vBIA. Furthermore, the topological approach outperforms the use of vBIA considering full connectivity in the whole range of the scenario. This fact highlights the importance of the topology in VLC networks and the capability of vBIA to adapt to partially connected VLC networks.

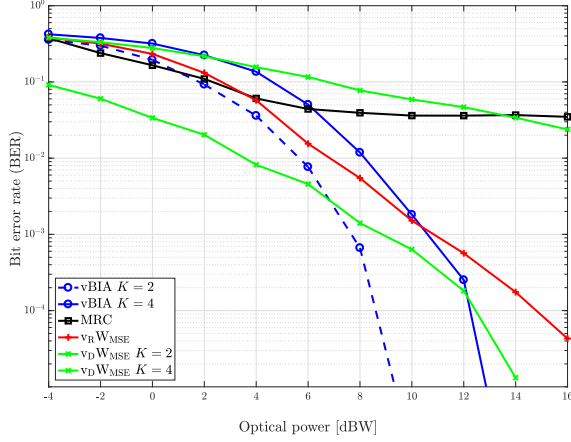The average user rate in the considered scenario B against

Fig. 22. BER for 2-PAM Modulation. Optical power transmitted 10 dBW.

Fig. 24. Achievable average user rate against cell radius for the considered scenario B. $K_p = 2$ and $K_{sh} = 2$.
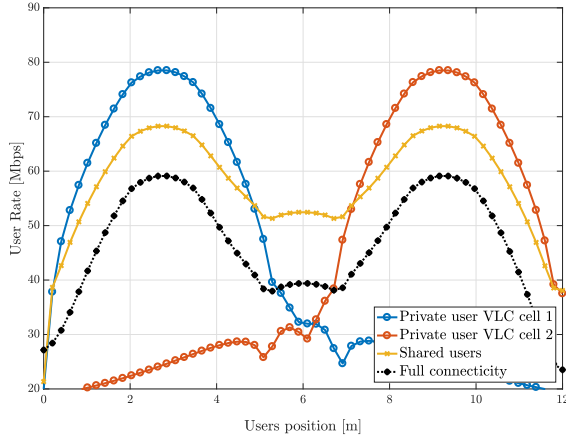

Fig. 23. User rate for vBIA in a homogeneous partially connected network. The performance assuming full connectivity is plotted for comparison purposes. Scenario B, $K_p = 2$ and $K_{sh} = 2$.

Fig. 25. CDF of the user rate for scenario A with $K = 4$ and scenario B with $K_p = 2$ and $K_{sh} = 2$.

cell radius is shown in Fig. 24. First, it can be seen that the average user rate decreases as the cell radius becomes smaller. For the vBIA scheme based on the network topology the average user rate outperforms other vBIA configurations. Notice that the lack of connectivity and the noise increase degrade considerably the performance of vBIA assuming full connectivity. On the other hand, allowing CCI between both VLC cells achieves greater average user rate than the full connectivity configuration. Furthermore, vBIA considering CCI outperforms $v_D W_{MSE}$ since only the users with the same index generate CCI when using vBIA [29]. Indeed, the performance of the $v_D W_{MSE}$ scheme decreases abruptly with the cell radius.

The cumulative distribution function (CDF) of the user rate for both scenarios is shown in Fig. 25. For the scenario A it can be seen that vBIA achieves a fair distribution ensuring a user rate between 50 Mbps and 90 Mbps. For $v_D W_{MSE}$, user rates above 90 Mbps are achievable for only the 30% of the users. However, notice that the 50% of the users achieve a rate below 50 Mbps. That is, high data rates can be achievable for specific
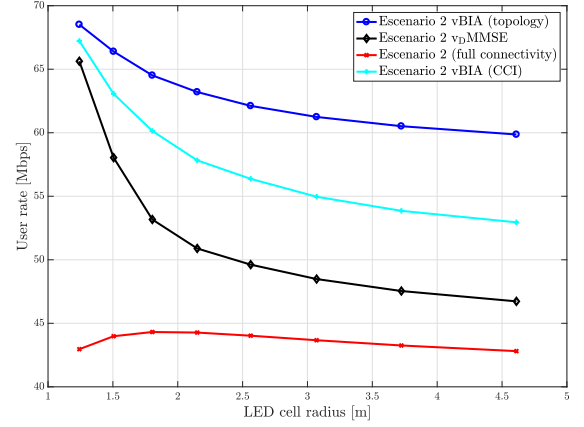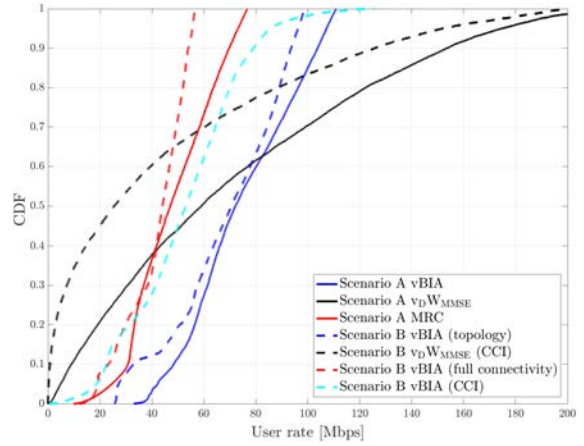
user distributions, but the properties of the optical channel lead to blackspot areas where the TPC schemes provide a low performance. As it is shown in previous simulations, the MRC scheme achieves a low performance in VLC systems since it is subject to intercell interference and management of the multi-user transmission. For the scenario B, the CCI plays a major role. In this sense, the user rate achieved by $v_D W_{MSE}$ suffers a considerable degradation in comparison with the performance obtained in scenario A. Furthermore, it can be seen that the use of vBIA schemes results suitable for VLC systems where the deployment of LED lights generate amorphous cells [6] depending on the connectivity of each user.

VIII. CONCLUSIONS

We propose the use of BIA schemes in VLC systems for aligning the interference without the need for CSIT or cooperation among the LED transmitters. A key ingredient to make this posible is the concept of a reconfigurable photodetector devised in this work. Beyond the benefits that BIA already provides for RF systems, it results suitable to

manage the particular constraints of the VLC systems such as the non-negativity of the transmitted signal, provide constant illumination or avoid the blackspot areas because of satisfying these constraints. Moreover, BIA is adaptable to practical VLC topologies from the user-centric perspective. Therefore, in contrast to multichannel techniques in absence of CSIT such as MRC, the BIA approach allows to manage the multi-user and intercell interference in VLC scenarios achieving multiplexing gain. In comparison to TPC schemes, the proposed BIA approach avoids the need for CSIT or cooperation among LED lights and it provides satisfactory achievable rates with a fair distribution and adequate BER.

References

[1] S. Wu, H. Wang, and C. H. Youn, "Visible light communications for 5g wireless networking systems: from fixed to mobile communications," *IEEE Network*, vol. 28, no. 6, pp. 41–45, Nov 2014.

[2] T. Komine and M. Nakagawa, "Fundamental analysis for visible-light communication system using led lights," *IEEE Transactions on Consumer Electronics*, vol. 50, no. 1, pp. 100–107, Feb 2004.

[3] C. X. Wang, F. Haider, X. Gao, X. H. You, Y. Yang, D. Yuan, H. M. Aggoune, H. Haas, S. Fletcher, and E. Hepsaydir, "Cellular architecture and key technologies for 5g wireless communication networks," *IEEE Communications Magazine*, vol. 52, no. 2, pp. 122–130, February 2014.

[4] J. Ding, Z. Xu, and L. Hanzo, "Accuracy of the point-source model of a multi-led array in high-speed visible light communication channel characterization," *IEEE Photonics Journal*, vol. 7, no. 4, pp. 1–14, Aug 2015.

[5] C. Chen, D. A. Basnayaka, and H. Haas, "Downlink performance of optical attocell networks," *Journal of Lightwave Technology*, vol. 34, no. 1, pp. 137–156, Jan 2016.

[6] R. Zhang, J. Wang, Z. Wang, Z. Xu, C. Zhao, and L. Hanzo, "Visible light communications in heterogeneous networks: Paving the way for user-centric design," *IEEE Wireless Communications*, vol. 22, no. 2, pp. 8–16, April 2015.

[7] L. Zeng, D. C. O'Brien, H. L. Minh, G. E. Faulkner, K. Lee, D. Jung, Y. Oh, and E. T. Won, "High data rate multiple input multiple output (MIMO) optical wireless communications using white led lighting," *IEEE Journal on Selected Areas in Communications*, vol. 27, no. 9, pp. 1654–1662, December 2009.

[8] Y. Hong, J. Chen, Z. Wang, and C. Yu, "Performance of a precoding MIMO system for decentralized multiuser indoor visible light communications," *IEEE Photonics Journal*, vol. 5, no. 4, pp. 7 800 211–7 800 211, Aug 2013.

[9] B. Li, J. Wang, R. Zhang, H. Shen, C. Zhao, and L. Hanzo, "Multiuser miso transceiver design for indoor downlink visible light communication under per-led optical power constraints," *IEEE Photonics Journal*, vol. 7, no. 4, pp. 1–15, Aug 2015.

[10] H. Marshoud, D. Dawoud, V. M. Kapinas, G. K. Karagiannidis, S. Muhaidat, and B. Sharif, "MU-MIMO precoding for VLC with imperfect CSI," in *Optical Wireless Communications (IWOW), 2015 4th Int. Workshop on*, Sept 2015, pp. 93–97.

[11] T. Fath and H. Haas, "Performance comparison of MIMO techniques for optical wireless communications in indoor environments," *IEEE Transactions on Communications*, vol. 61, no. 2, pp. 733–742, February 2013.

[12] S. A. Jafar, "Blind interference alignment," *IEEE Journal of Selected Topics in Signal Processing*, vol. 6, no. 3, pp. 216–227, June 2012.

[13] T. Gou, C. Wang, and S. A. Jafar, "Aiming perfectly in the dark-blind interference alignment through staggered antenna switching," *IEEE Transactions on Signal Processing*, vol. 59, no. 6, pp. 2734–2744, June 2011.

[14] M. M. Cespedes, J. Plata-Chaves, A. G. Armada, and L. Vandendorpe, "A blind interference alignment scheme for practical channels," in *2016 IEEE International Conference on Communications (ICC)*, May 2016, pp. 1–6.

[15] J. Costantine, Y. Tawk, S. E. Barbin, and C. G. Christodoulou, "Reconfigurable antennas: Design and applications," *Proceedings of the IEEE*, vol. 103, no. 3, pp. 424–437, March 2015.

[16] S. Begashaw, J. Chacko, N. Gulati, D. H. Nguyen, N. Kandasamy, and K. R. Dandekar, "Experimental evaluation of a reconfigurable antenna system for blind interference alignment," in *2016 IEEE 17th Annual Wireless and Microwave Technology Conference (WAMICON)*, April 2016, pp. 1–6.

[17] M. Morales-Cespedes, J. Plata-Chaves, D. Toumpakaris, S. A. Jafar, and A. G. Armada, "Blind interference alignment for cellular networks," *IEEE Transactions on Signal Processing*, vol. 63, no. 1, pp. 41–56, Jan 2015.

[18] ——, "Cognitive blind interference alignment for macro-femto networks," *IEEE Transactions on Signal Processing*, vol. PP, no. 99, pp. 1–1, 2017.

[19] J. M. Kahn and J. R. Barry, "Wireless infrared communications," *Proceedings of the IEEE*, vol. 85, no. 2, pp. 265–298, Feb 1997.

[20] J. Grubor, S. Randel, K. D. Langer, and J. W. Walewski, "Broadband information broadcasting using led-based interior lighting," *Journal of Lightwave Technology*, vol. 26, no. 24, pp. 3883–3892, Dec 2008.

[21] J. B. Wang, Q. S. Hu, J. Wang, M. Chen, and J. Y. Wang, "Tight bounds on channel capacity for dimmable visible light communications," *Journal of Lightwave Technology*, vol. 31, no. 23, pp. 3771–3779, Dec 2013.

[22] V. Jungnickel, V. Pohl, S. Nonnig, and C. von Helmolt, "A physical model of the wireless infrared communication channel," *IEEE Journal on Selected Areas in Communications*, vol. 20, no. 3, pp. 631–640, Apr 2002.

[23] Y. Wang, X. Wu, and H. Haas, "Load balancing game with shadowing effect for indoor hybrid lifi/rf networks," *IEEE Transactions on Wireless Communications*, vol. 16, no. 4, pp. 2366–2378, April 2017.

[24] S. H. Yang, E. M. Jung, and S. K. Han, "Indoor location estimation based on led visible light communication using multiple optical receivers," *IEEE Communications Letters*, vol. 17, no. 9, pp. 1834–1837, September 2013.

[25] A. Nuwanpriya, S. W. Ho, and C. S. Chen, "Indoor MIMO visible light communications: Novel angle diversity receivers for mobile users," *IEEE Journal on Selected Areas in Communications*, vol. 33, no. 9, pp. 1780–1792, Sept 2015.

[26] S. Zhang, S. Watson, J. J. D. McKendry, D. Massoubre, A. Cogman, E. Gu, R. K. Henderson, A. E. Kelly, and M. D. Dawson, "1.5 gbit/s multi-channel visible light communications using cmos-controlled gan-based leds," *Journal of Lightwave Technology*, vol. 31, no. 8, pp. 1211–1216, April 2013.

[27] J. R. Barry and J. M. Kahn, "Link design for nondirected wireless infrared communications," *Appl. Opt.*, vol. 34, no. 19, pp. 3764–3776, Jul 1995.

[28] H. Yang, W. Shin, and J. Lee, "Hierarchical blind interference alignment over interference networks with finite coherence time," *IEEE Transactions on Signal Processing*, vol. 64, no. 5, pp. 1289–1304, March 2016.

[29] C. Wang, H. C. Papadopoulos, S. A. Ramprashad, and G. Caire, "Improved blind interference alignment in a cellular environment using power allocation and cell-based clusters," in *2011 IEEE International Conference on Communications (ICC)*, June 2011, pp. 1–6.

[30] S. Nakamura and M. R. Krames, "History of gallium-nitride-based light-emitting diodes for illumination," *Proceedings of the IEEE*, vol. 101, no. 10, pp. 2211–2220, Oct 2013.

[31] R. Jain, D. Chiu, and W. Hawe, "A quantitative measure of fairness and discrimination for resource allocation in shared computer systems," *CoRR*, vol. cs.NI/9809099, 1998. [Online]. Available: http://arxiv.org/abs/cs.NI/9809099

Máximo Morales Céspedes (S'10-M'15) was born in Valdepeñas, C. Real, Spain, in 1986. He received the B.Sc., and M.Sc., and Ph.D. degrees from the Universidad Carlos III de Madrid, Spain, in 2010, 2012, 2015, respectively, all in electrical engineering, with a specialization in Multimedia and Communications. In 2012 he was finalist of the IEEE Region 8 Student Paper Contest. From 2015 to 2017 he has been working as a postdoctoral fellow with the Institute of Information and Communication Technologies, Electronics and Applied Mathematics (ICTEAM) at Universite Catholique de Louvain. Currently, he is with the Department of Signal Theory and Communications, Universidad Carlos III de Madrid, Spain. His research interests are interference management, hardware implementations, MIMO techniques and signal processing applied to wireless communications.

Martha Cecilia Paredes Paredes (S'12-M'15) received her Eng. degree from Escuela Politécnica Nacional (EPN), Quito, Ecuador in 2008, the M.Sc. and Ph.D of Multimedia and Communications from Carlos III University of Madrid, Spain in 2010 and 2014, respectively. Also, from 2010 to 2011 she worked as an Assistant Lecturer at Universidad de las Américas (UDLA), Quito - Ecuador. She is currently an Assistant Professor at Departamento de Electrónica, Telecomunicaciones y Redes de Información (DETRI), EPN, Quito, Ecuador. Her research interests include multicarrier communications, OFDM transmissions, 5G networks, and signal processing for wireless communications.

Ana García Armada (S'96–A'98–M'00–SM'08) received the Ph.D. degree in electrical engineering from the Polytechnical University of Madrid in February 1998. She is currently Professor at University Carlos III of Madrid, Spain, where she has occupied a variety of management positions (Head of Signal Theory and Communications Department, Vice-dean of Electrical Engineering, Deputy Vice-Chancellor of International Relations, among others). She is leading the Communications Research Group at this university. She has been visiting scholar at Stanford University, Bell Labs and University of Southampton. She has participated in more than 30 national and 10 international research projects as well as 20 contracts with the industry, all of them related to wireless communications. She is the co-author of eight book chapters on wireless communications and signal processing. She has published around 150 papers in international journals and conference proceedings and she holds four patents. She has contributed to international standards organizations such as ITU and ETSI and is member of the expert group of the European 5G PPP. She serves on the editorial boards of Physical Communication, IET Communications and IEEE Communications Letters. She has received a Young Researchers Excellence Award and an Award to Best Practices in Teaching, both from University Carlos III of Madrid, Her main interests are multi-carrier and multi-antenna techniques and signal processing applied to wireless communications.

Luc Vandendorpe (M'93–SM'99–F06) was born in Mouscron, Belgium, in 1962. He received the degree (summa cum laude) in electrical engineering and the Ph.D. degree from the Universit Catholique de Louvain (UCLouvain), Louvain La Neuve, Belgium, in 1985 and 1991, respectively. Since 1985, he has been UCLouvain, where he ?rst worked in the ?eld of bit rate reduction techniques for video coding. In 1992, he was a Visiting Scientist at TUDelft. From October 1992 to August 1997, he was a Senior Research Associate of the Belgian NSF, UCLouvain, and an invited Assistant Professor. He is now a Full Professor with the Institute for Information and Communication Technologies, Electronics, and Applied Mathematics, UCLouvain. His research interests include digital communication systems and more precisely resource allocation for OFDM(A)-based multicell systems, MIMO and distributed MIMO, sensor networks, UWB-based positioning, and wireless power transfer. He is and has been a TPC Member for numerous IEEE conferences (VTC, Globecom, SPAWC, ICC, PIMRC, and WCNC). He was a Co-Technical Chair for the IEEE ICASSP 2006. He served as an Editor for Synchronization and Equalization of the IEEE TRANSACTIONS ON COMMUNICATIONS between 2000 and 2002, and as an Associate Editor of the IEEE TRANSACTIONS ON WIRELESS COMMUNICATIONS between 2003 and 2005, and the IEEE TRANSACTIONS ON SIGNAL PROCESSING between 2004 and 2006. He was the Chair of the IEEE Benelux joint chapter on communications and vehicular technology between 1999 and 2003. He was an elected member of the Signal Processing for Communications Committee between 2000 and 2005, and an elected member of the Sensor Array and Multichannel Signal Processing Committee of the Signal Processing Society between 2006 and 2008, and between 2009 and 2011. Luc Vandendorpe is a Fellow of the IEEE.